

Non-homogeneous thermal transport in graphene disk at the micro/nano scale

Chuang Zhang^a, Dengke Ma^{a,b}, Zhaoli Guo^{a,*}, Nuo Yang^{a,b,*}

^aState Key Laboratory of Coal Combustion, Huazhong University of Science and Technology, Wuhan, 430074, China

^bNano Interface Center for Energy (NICE), School of Energy and Power Engineering, Huazhong University of Science and Technology (HUST), Wuhan 430074, People's Republic of China

Abstract

A novel non-homogeneous or graded thermal conductivity along the radius direction in a single graphene disk structure has been predicted in previous study by using classical non-equilibrium molecular dynamics method. However, the size of the simulated system was only up to 25 nm due to the limitation of computational method. So whether the graded thermal conductivity phenomena can be observed over hundreds of nanometers is an open question need to be answered. In this work, the thermal conductivity of graphene disk is studied from nano scale up to micro scale based on the phonon Boltzmann transport equation (BTE) under Callaway's dual relaxation model. The results show that the graded thermal conductivity phenomena exist along the radius direction as the disk size increases from hundreds of nanometers to tens of microns. In the ballistic regime, the numerical results are in excellent agreement with our derived analytical solutions. As the system size is much larger than the phonon mean free path, the moment conservation normal (N) scattering leads to a diverging thermal conductivity and generates a drift velocity along the radius direction nearly inversely proportional to the radius. It is different from the moment destroying resistive (R) scattering which recovers the traditional Fourier's law of thermal conduction. Furthermore, as the system size increases, the graded rate of the thermal conductivity increases for N scattering but decreases for R scattering.

Keywords: multiscale heat transfer, Callaway model, graphene disk, non-homogeneous thermal conductivity, N or R scattering

1. Introduction

For the heat transfer in three dimensional bulk homogeneous materials, the traditional Fourier's law of thermal conduction [1] is widely used. However, as the size or dimension of the thermal system decreases, the Fourier's law of thermal conduction is not capable of describing the multiscale thermal transport phenomena correctly [2, 3, 4, 5]. The main reason is that the predominant heat carrier in solid materials [6], namely, phonon, no longer transports diffusively in these regimes. On the one hand, as the system size is smaller than

*Corresponding author

Email addresses: zhangcmzt@hust.edu.cn (Chuang Zhang), dengke@hust.edu.cn (Dengke Ma), zlguo@hust.edu.cn (Zhaoli Guo), nuo@hust.edu.cn (Nuo Yang)

or comparable to the phonon mean free path, the phonon boundary scattering becomes strong and impedes the phonon transport so that the thermal conductivity decreases significantly, [2, 3] which has been validated by both experimental measurements and numerical simulations [7, 8, 9]. The thermal conductivity can be decreased by adjusting the geometrical shape or arrangement of the nano-porous structures [10, 11, 12]. Since the phonon boundary scattering is influenced significantly by the surface structure and roughness, especially in the ballistic regime. Furthermore, as the system size is close or comparable to the phonon wave length, the phonon dispersion may be modified [8, 9] and the phonon wave nature is non-negligible [13] so that the physical parameters in the bulk regime are invalid. On the other hand, for some low dimensional materials, the phonon scattering mechanisms are more complicated than that in bulk materials [14, 15, 16]. For example, in graphene [17, 18], the momentum conservation normal (N) scattering is non-negligible compared to the momentum destroying resistive (R) scattering [15, 19]. Different from the R scattering which recovers the Fourier's law of thermal conduction in the diffusive regime, the N scattering causes no thermal resistance. In addition, the strong N scattering may result in some novel heat transfer phenomena such as second sound and phonon poiseuille flow [19, 20]. Some studies also show that the thermal conductivity in the low-dimensional system diverges with the system size L [21, 4, 22], which is also a striking example of traditional Fourier's law of thermal conduction.

Many previous work focuses on studying length-dependent thermal conductivity of the materials, however, the spatial dependent thermal conductivity for a given length scale also affects phonon transport significantly. As we all known, the bulk thermal conductivity is generally dependent of the temperature [2, 3]. Actually, if the temperature in the domain is over a large range, the thermal conductivity will not be a constant and the temperature distribution will be nonlinear [23, 24].

Apart from the large temperature difference, the material anisotropy can also lead to spatial dependent thermal conductivity even under the small temperature difference. One of these is the functionally graded material (FGM) [25, 26] consisting of two or more phases. The thermal properties can be adjusted by taking advantage of desirable features of different constituent phases. For example, the spatial dependent thermal conductivity can be achieved by inhomogeneous doping [26, 27], which influences both the phonon dispersion and scattering. Another approach is the single homogeneous materials but with asymmetric geometries, which are widely used in thermal rectification [28, 29, 30]. Previous studies based on the molecular dynamics simulations show that in asymmetric graphene ribbons the heat flux runs preferentially along the direction of decreasing width [31]. Other work based on the Monte Carlo method also shows that thermal conduction can be influenced by changing the cross-session of the silicon nanowires [32]. The tapered cross-section nanowires can decelerate thermal flux.

The non-homogeneous thermal transport has also been found in single symmetry graphene disk based on molecular dynamics [33]. Numerical results show that at steady state the thermal conductivity along the radius direction is approximately linear to the power of the radius r^α , where α is the graded rate

and r is the distance to the center of the circle. The closer the atoms to the disk center, the smaller the thermal conductivity is. Similar graded thermal conductivity phenomena are also founded in carbon nanocone [34]. However, due to the limitation of computational resources, previous studies about the graded thermal conductivity are limited in tens of nanometers.

In this work, we focus on the thermal transport along the radius direction at steady state in graphene disk from hundreds of nanometers to tens of microns. Instead of the molecular dynamics simulations [33, 34], the stationary phonon Boltzmann transport equation (BTE) is used, which is a powerful tool to study the multiscale heat transfer problems [6]. The Callaway model [15, 19, 35] is used, which contains both the momentum conservation N scattering and momentum destroying R scattering and predicts the thermal conductivity of graphene well.

2. Structure and phonon BTE

Giving an isotropic graphene disk [33], as shown in Fig. 1, the radii of the inner and outer circles are l and L , respectively. The inner circle is the hot red area with a fixed temperature $T_h = T_0 + \Delta T/2$, and the temperature of the outer circle is $T_c = T_0 - \Delta T/2$. In order to avoid the thermal rectification [28, 29], we control the temperature difference in the domain be very small, i.e., $\Delta T/T_0 = 0.01$. Due to symmetry, the thermal conductivity along the radius direction $k(r)$ can be calculated by

$$\begin{aligned} k(r) &= -\frac{\mathbf{q} \cdot \mathbf{n}}{dT/dr} \\ &= -\frac{Q(r)}{2\pi r (dT/dr)} \\ &= -\frac{Q(r)}{2\pi (dT/d(\ln r))}, \end{aligned} \tag{1}$$

where r is the distance to the center of the graphene disk, $l \leq r \leq L$, \mathbf{q} is the heat flux, $Q(r) = 2\pi r \mathbf{q} \cdot \mathbf{n}$ is the total heat flux across the circle with radius r , \mathbf{n} is the normal unit vector along the radius direction from the inner circle to the outer circle. At steady state, Q is a constant due to the energy conservation. In what follows, we set $T_0 = 300K$ and $l/L = 0.2$.

To study the heat transfer phenomena at the micro/nano scale at steady state in graphene disk, the stationary phonon BTE under Callaway's dual relaxation model [36, 19, 15] is used, which contains the momentum conservation N scattering and the moment destroying R scattering. The model was validated to predict the thermal conductivity of graphene well in a wide range [19, 15, 37]. The details of the Callaway model and the associated boundary conditions are discussed in Appendix A. The implicit discrete ordinate method (DOM) [38, 39, 40] is used to solve the model equation, which can refer to Ref [35].

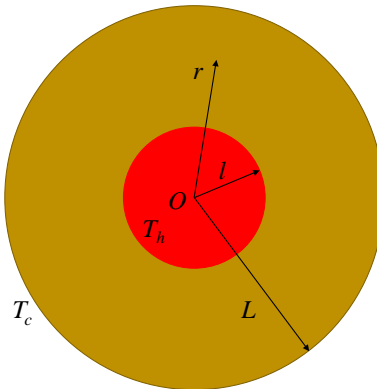


Figure 1: Geometry of the graphene disk.

3. Results and discussions

3.1. Heat transfer in graphene disk

The thermal transport in graphene disk is simulated accounting for the phonon dispersion and polarization [41, 42, 43, 44, 45] (appendix B), which will be the combined results of all different phonon scattering mechanisms.

Figure 2 shows the temperature and thermal conductivity distributions along the radius direction in graphene disk with different system sizes $2L$, where $r^* = \lg(r/l) / \lg(L/l)$, $T^* = (T - T_c) / \Delta T$, $k^* = k/k_0$, $k_0 = \frac{1}{2} \sum_p \int (C|\mathbf{v}|^2 \tau) d\omega$. As the system size is 100nm, there are rare N and R scattering and the phonon boundary scattering dominates the heat transfer. It can be observed that the temperature profiles come close to the analytical solutions in the ballistic regime, i.e., Eq. (20) (appendix C), as shown in Fig. 2a. The distribution of the thermal conductivity (Fig. 2b) is consistent with the analytical solutions derived in Eq. (22), too. As the size increases, the boundary scattering becomes weak and the intrinsic phonon-phonon scattering controls the heat transfer so that the temperature slip decreases near the boundaries and the temperature profiles come to linear. From Fig. 2b, it can also be observed that the thermal conductivity along the radius direction is dependent of the radius from hundreds of nanometers to tens of microns. The closer to the inner circle, the smaller the thermal conductivity. This phenomena are similar to the results predicted at several nanometers by MD [33].

What's different is that for a given system size the graded rate of thermal conductivity α is dependent of the radius if ignoring the numerical fluctuations, as shown in Fig. 3, where

$$\alpha = \frac{\partial (\lg k^*)}{\partial r^*}. \quad (2)$$

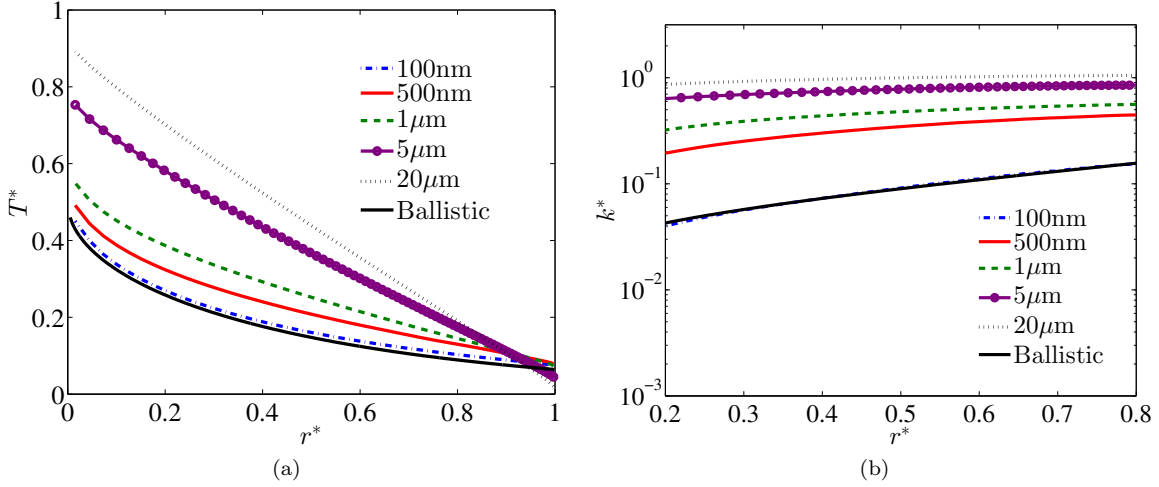


Figure 2: Macroscopic distributions in graphene disk along radius direction. The normalized coordination is $r^* = \lg(r/l) / \lg(L/l)$. (a) Temperature distribution, where $T^* = (T - T_c) / \Delta T$. In the ballistic regime, analytical solutions of temperature are derived, i.e., Eq. (20). (b) Normalized graded thermal conductivity k^* , where $k^* = k/k_0$, $k_0 = \frac{1}{2} \sum_p \int (\tau C |\mathbf{v}|^2 \tau) d\omega$. 'Ballistic' is the thermal conductivity calculated by the analytical solutions derived in Eq. (22) with $2L = 100$ nm.

It can be observed that the graded rate decreases as the radius increases from $r^* = 0.2$ to $r^* = 0.8$, which is similar to that predicted by the analytical solutions in the ballistic regime, i.e., Eq. (19). Based on Eq. (19), the radius dependent graded rate is related to the radii of the inner and outer circles. In other words, the phonon boundary scattering affects the distribution of the graded rate to some extent. As the system size increases from hundreds of nanometers to tens of microns, the graded rate of the thermal conductivity decreases gradually and tends to zero for a given r^* . That's because although the N scattering causes no thermal resistance [19], the boundary scattering and R scattering are momentum destroying and cause large thermal resistance. As the system size is much larger than the phonon mean free path, the dominated momentum destroying scattering finally leads to a converged thermal conductivity with $\alpha = 0$.

Figure 4 shows the normalized drift velocity along the radius direction, where $u^* = \frac{|\mathbf{u}|T_0}{\Delta T V_a}$, $V_a = \left(\sum_p \int C |\mathbf{v}| d\omega \right) \left(\sum_p \int C d\omega \right)^{-1}$ is the average group velocity. Different from previous studies [46, 47, 20] in which the drift velocity is a constant, our results show that the drift velocity along the radius direction is dependent of the radius. As size increases, the phonon boundary scattering becomes weak but both the N and R scattering start to play a role on heat transfer. It can be observed that the drift velocity increases first and then decreases gradually as the size increases from 100 nm to 20μm, which is the combined results of the N, R and boundary scattering. In order to deeply understand the effects of different phonon scattering mechanisms, we have to separate them, which will be discussed in the next subsection. As $2L = 20\mu\text{m}$, the drift velocity is very small, which indicates that in this regime the momentum destroying scattering dominates the phonon transport and restores the phonon distribution close to f_R^{eq} .

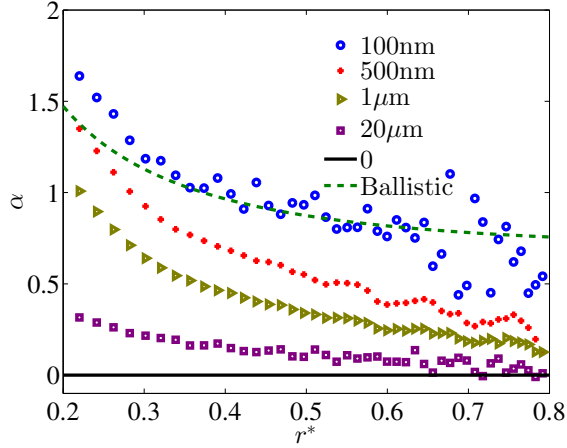


Figure 3: The distribution of α along the radius direction at different system size $2L$. In the ballistic regime, the analytical solutions are derived in Eq. (19).

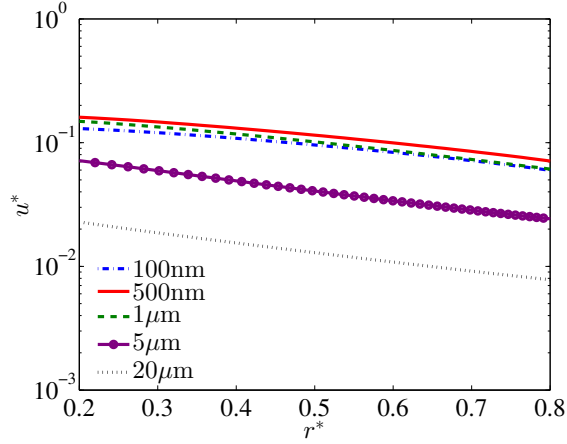


Figure 4: Normalized drift velocity along the radius direction with different length scales, where $u^* = \frac{|\mathbf{u}|T_0}{\Delta T V_a}$, $V_a = \left(\sum_p \int C|\mathbf{v}|d\omega\right) \left(\sum_p \int C d\omega\right)^{-1}$. The normalized coordination is $r^* = \lg(r/l) / \lg(L/l)$.

3.2. Thermal effects of N or R scattering

The above results show that in graphene, both the N scattering and R scattering play an important role on heat transfer in different regimes [48, 15, 19, 49]. In order to understand their separate effects on the thermal transport in graphene disk, two following cases are simulated:

1. all phonon-phonon scattering is momentum destroying R scattering, i.e., $\tau_N^{-1} = 0$;
2. all phonon-phonon scattering is momentum conservation N scattering, i.e., $\tau_R^{-1} = 0$.

In this subsection the phonon dispersion is not included and we set $|\mathbf{v}| = \omega/|\mathbf{K}|$ for simplicity. Then the heat transfer is mainly decided by the Knudsen number, which is the ratio of the phonon mean free path to the system size and defined as $\text{Kn} = |\mathbf{v}|\tau/2L$.

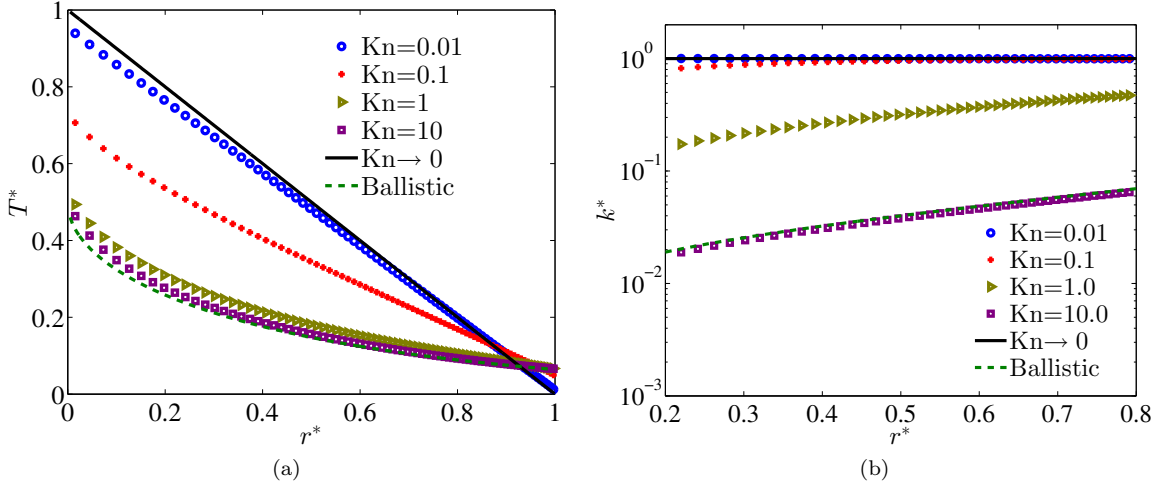


Figure 5: Macroscopic distributions along the radius direction with different Knudsen numbers when all phonon-phonon scattering is R scattering, i.e., $\tau_N^{-1} = 0$. The normalized coordination is $r^* = \lg(r/l) / \lg(L/l)$. (a) Normalized temperature field, $T^* = (T - T_c) / \Delta T$. Analytical solutions as $Kn \rightarrow 0$ or in the ballistic regime are derived in the Appendix C, i.e., Eq. (25) and Eq. (16). (b) Normalized thermal conductivity $k^* = k/k_0$, $k_0 = \frac{1}{2} \sum_p \int (\tau C |v|^2 \tau) d\omega$. 'Ballistic' is the thermal conductivity calculated by the analytical solutions derived in Eq. (18) with $Kn = 10.0$.

3.2.1. Only R scattering

Figure 5a shows the temperature distributions along the radius direction when all phonon-phonon scattering is R scattering. As $Kn = 0.01$, the temperature profiles come to linear, which are consistent with the analytical solutions with $Kn \rightarrow 0$, as shown in Eqs. (25) and (26) in Appendix C. Because in this regime, the R scattering dominates the heat transfer and recovers the traditional Fourier's law of thermal conduction correctly. With the increasing of the Knudsen number, the phonon boundary scattering plays an important role and the non-diffusive phonon transport happens, which leads to the temperature slip near the boundaries. As $Kn = 10.0$, phonon scattering rarely happens and the heat transfer is in the ballistic regime. The boundary scattering dominates the thermal transport and the numerical profiles are consistent with the analytical solutions derived in Eq. (16) in Appendix C.

Figure 5b shows the distribution of the normalized thermal conductivity k^* along the radius direction. It can be observed that as Kn increases, the thermal conductivity decreases for a given r . Furthermore, the thermal conductivity along the radius direction is no longer a constant as $Kn \geq 0.1$. The smaller the r is, the smaller the thermal conductivity is. Because near the boundaries, the phonon boundary scattering leads to highly non-equilibrium phonon transport and increases the thermal resistance. Compared to the outer circle, the radius of the inner circle is smaller so that there is stronger phonon boundary scattering. In other words, the local Knudsen number close to the inner circle is larger. As r increases, the chance of local phonon scattering with inner boundaries decreases so that the thermal conductivity increases. In the ballistic regime, for example as $Kn = 10.0$, the simulated radius dependent thermal conductivity is consistent with the analytical solutions as derived in Eq. (18).

Figure 6 shows the distributions of the graded rate α along the radius direction at different Knudsen

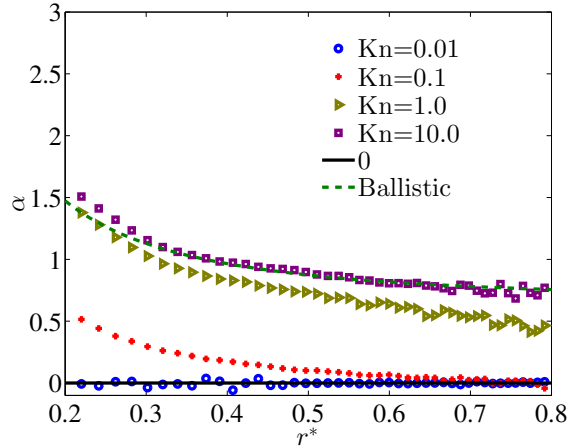


Figure 6: The distribution of α along the radius direction at different Knudsen numbers as $\tau_N^{-1} = 0$. In the ballistic limit, the analytical solutions are derived in Eq. (19).

numbers. It can be found that generally, as r^* increases from 0.2 to 0.8, α decreases for a given Knudsen number if ignoring the fluctuations. As $\text{Kn} = 10.0$, the numerical results are in good agreement with our analytical solutions derived in Eq. (19). As Kn decreases from 10.0 to 0.01, the momentum destroying R scattering dominates the heat transfer and α decreases gradually and goes to 0.

3.2.2. Only N scattering

When all phonon-phonon scattering is momentum conservation N scattering, the heat transfer is something different. As the Kn decreases, the N scattering dominates the heat transfer and the temperature along the radius direction goes to a constant, as shown in Fig. 7a. As $\text{Kn} = 0.01$, the temperature distribution is almost overlapping with the analytical solution with $\text{Kn} \rightarrow 0$ derived in Eq. (32). At the same time, the thermal conductivity increases significantly with the increasing of the system size, as shown in Fig. 7b. Theoretically, the momentum conservation scattering leads to an infinite thermal conductivity if ignoring the boundary scattering. Furthermore, from Fig. 8, it can be observed that the graded rate α increases as Kn decreases from 10.0 to 0.1, which is different from that observed in Fig. 6 mentioned in the last subsection. While in the ballistic regime, the thermal phenomena are similar and consistent with the analytical solutions due to the rare phonon-phonon scattering.

Different from the R scattering, the N scattering will generate a nonzero drift velocity. As shown in Fig. 9, the numerical profiles of the drift velocity along the radius direction are nearly linear and parallel to each other at different Knudsen numbers, where $u^* = \frac{|\mathbf{u}|T_0}{|v|\Delta T}$ is the normalized drift velocity along the radius. Based on the momentum conservation of the N scattering (Eq. (13)) and frequency-independent assumption, if

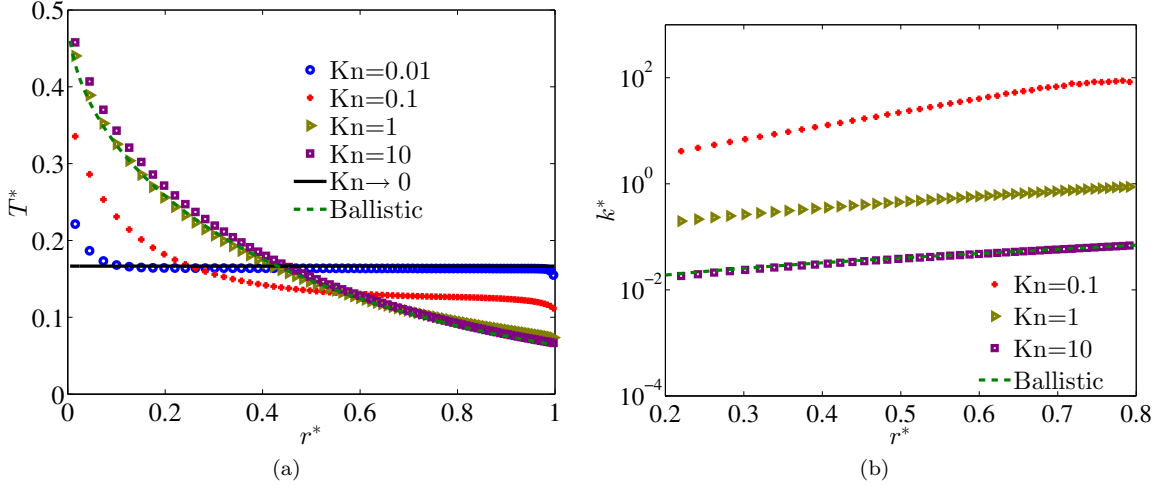


Figure 7: Macroscopic distributions along the radius direction with different Knudsen numbers when all phonon-phonon scattering is N scattering, i.e., $\tau_R^{-1} = 0$. The normalized coordination is $r^* = \lg(r/l) / \lg(L/l)$. (a) Normalized temperature field, $T^* = (T - T_c) / \Delta T$. Analytical solutions with $\text{Kn} \rightarrow 0$ or in the ballistic regime are derived in the Appendix C, i.e., Eq. (32) and Eq. (16). (b) Normalized thermal conductivity $k^* = k/k_0$, where $k_0 = \frac{1}{2} \sum_p \int (\tau C |\mathbf{v}|^2 \tau) d\omega$. 'Ballistic' is the thermal conductivity calculated by the analytical solutions derived in Eq. (18) with $\text{Kn} = 10.0$.

ignoring the boundary scattering, we have

$$\begin{aligned}
 Q(r) &= 2\pi r \mathbf{n} \cdot \int_{2\pi} \mathbf{v} f d\Omega \\
 &= 2\pi r \mathbf{n} \cdot \int_{2\pi} \mathbf{v} f_N^{eq} d\Omega \\
 &= r\pi C T(r) |\mathbf{u}(r)| \\
 &\approx r\pi C T_0 |\mathbf{u}(r)| \\
 &= \text{constant},
 \end{aligned} \tag{3}$$

$$\implies |\mathbf{u}(r)| \propto r^{-1}. \tag{4}$$

Actually as $\text{Kn} \rightarrow 0$, we mathematically prove that the drift velocity is inversely proportional to the radius, as shown in Eq. (33). From the profiles, it can also be observed that our analytical solutions keep well with the numerical results with $\text{Kn} = 0.01$. As the Knudsen number increases, the boundary scattering becomes stronger and stronger which restores the distribution function to f_R^{eq} with zero drift velocity so that the drift velocity decreases.

4. Conclusion

In this work, the thermal transport in graphene disk is studied at micro/nano scale by using the stationary phonon Boltzmann transport equation under Callaway's dual relaxation model. Numerical results are in good agreement with our derived analytical solutions in the ballistic regime. As the disk size increases from hundreds of nanometers to tens of microns, the radius dependent thermal conductivity phenomena

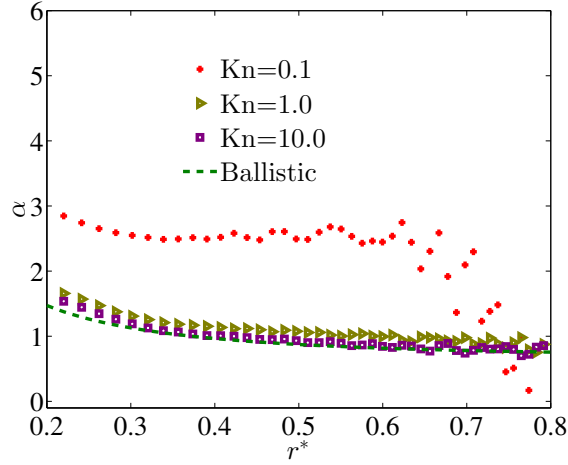


Figure 8: The distribution of α along the radius direction at different Knudsen numbers as $\tau_R^{-1} = 0$. In the ballistic regime, the analytical solutions are derived in Eq. (19).

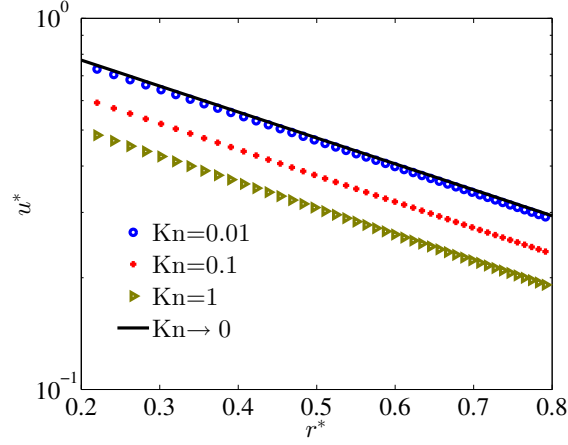


Figure 9: Normalized drift velocity along the radius direction with different Knudsen numbers when all phonon-phonon scattering is N scattering, i.e., $\tau_R^{-1} = 0$, where $u^* = \frac{|u|T_0}{|v|\Delta T}$ is the normalized drift velocity along the radius. The normalized coordination is $r^* = \lg(r/l) / \lg(L/l)$. Analytical solutions with $\text{Kn} \rightarrow 0$ are given in Eq. (33)

still exist and the graded rate decreases gradually till 0. The closer to the center, the smaller the thermal conductivity. Furthermore, if look at the overall trend, the graded rate of the thermal conductivity decreases as the radius increases for a given system size. For R scattering, as the system size increases, the graded rate decreases till 0 and the heat transfer recovers the traditional Fourier's law of thermal conduction. But for N scattering, the graded rate increases and the thermal conductivity goes to infinite with the increasing of the system size. In addition, the N scattering generates a drift velocity along the radius direction nearly inversely proportional to the radius. The present results show that even far beyond the molecular dynamics simulation scale [33, 34], the heat transfer in the graphene disk is still non-homogeneous.

APPENDIX A: Callaway model

The mathematical formula of stationary phonon BTE under Callaway's dual relaxation model [19, 15, 35] is

$$\mathbf{v} \cdot \nabla f = \frac{f_R^{eq} - f}{\tau_R} + \frac{f_N^{eq} - f}{\tau_N}, \quad (5)$$

where $f = f(\mathbf{x}, \mathbf{K}, \omega, p)$ is the phonon distribution function, \mathbf{x} is the physical position, \mathbf{K} is the wave vector in 2D space and assumed to be isotropic, i.e., $\mathbf{K} = |\mathbf{K}|\mathbf{s}$, \mathbf{s} is the unit direction vector, ω is the angular frequency, $\mathbf{v} = \nabla_{\mathbf{K}}\omega$ is the group velocity, p is the phonon polarization (see appendix B). The left term of Eq. (5) represents the phonon advection and the right is the phonon scattering term [50], which is composed of two parts: the first part is the momentum destroying R scattering and the second part is the momentum conservation N scattering [19, 15, 35]. The former relaxes the distribution function to the equilibrium state f_R^{eq} with relaxation time τ_R and the latter relaxes to the displaced equilibrium distribution f_N^{eq} with relaxation time τ_N [46, 19, 15], where

$$f_R^{eq}(T) \approx C(\omega, p, T_0) (T - T_0) / 2\pi, \quad (6)$$

$$f_N^{eq}(T, \mathbf{u}) \approx C(\omega, p, T_0) (T - T_0) / 2\pi + C(\omega, p, T_0) T \frac{\mathbf{K} \cdot \mathbf{u}}{2\pi\omega}, \quad (7)$$

where T is the temperature and \mathbf{u} is the drift velocity. $C(\omega, p, T_0)$ is the mode specific heat at T_0 , i.e.,

$$C(\omega, p, T_0) = \frac{\partial f_{BE}(T_0)}{\partial T} \hbar\omega D(\omega, p), \quad (8)$$

where $f_{BE}(T) = (\exp(\hbar\omega/k_B T) - 1)^{-1}$ is the Bose-Einstein distribution [6], k_B and \hbar are the Boltzmann constant and Plack constant reduced by 2π , $D(\omega, p) = |\mathbf{K}| / (2\pi|\mathbf{v}|)$ is the phonon density of state [14, 51, 17]. The temperature T and heat flux \mathbf{q} can be updated by taking the moment of the distribution function, i.e.,

$$T = T_0 + \frac{\sum_p \int \int_{2\pi} f d\Omega d\omega}{\sum_p \int C d\omega}, \quad (9)$$

$$\mathbf{q} = \sum_p \int \int_{2\pi} \mathbf{v} f d\Omega d\omega, \quad (10)$$

where $d\Omega$ and $d\omega$ are the integral over the whole 2D solid angle space and frequency space. Based on the energy conservation of N and R scattering, we have

$$0 = \sum_p \int \int_{2\pi} \frac{f_N^{eq} - f}{\tau_N} d\Omega d\omega, \quad (11)$$

$$0 = \sum_p \int \int_{2\pi} \frac{f_R^{eq} - f}{\tau_R} d\Omega d\omega. \quad (12)$$

In addition, the N scattering satisfies the momentum conservation, i.e.,

$$0 = \sum_p \int \int_{2\pi} \frac{\mathbf{K}}{\omega} \frac{f_N^{eq} - f}{\tau_N} d\Omega d\omega. \quad (13)$$

The boundary conditions are also indispensable for the solutions of the phonon BTE [50]. In graphene disk, the thermalizing boundary condition is used to deal with the isothermal boundaries with a fixed wall temperature T_w , i.e.,

$$f(\mathbf{x}_b, \mathbf{s}) = f_R^{eq}(T_w), \quad \mathbf{s} \cdot \mathbf{n}_b > 0, \quad (14)$$

where \mathbf{n}_b is the normal unit vector of the boundary \mathbf{x}_b pointing to the computational domain.

APPENDIX B: Phonon dispersion and scattering in graphene

In graphene, there are six phonon polarizations including three acoustic ones and three optical ones [52, 44, 45, 53]. We only consider the phonon acoustic polarizations and assume that the wave vector space is isotropic. The phonon dispersion curves [44, 45] for each phonon branch are shown as follows: for LA, $\omega = c_{LA}|\mathbf{K}|$, $c_{LA} = 2.13 \times 10^4 \text{m/s}$, for TA, $\omega = c_{TA}|\mathbf{K}|$, $c_{TA} = 1.36 \times 10^4 \text{m/s}$, for ZA, $\omega = c_{ZA}|\mathbf{K}|^2$, $c_{ZA} = 6.2 \times 10^{-7} \text{m}^2/\text{s}$, where $0 \leq |\mathbf{K}| \leq 1.5 \times 10^{10} \text{m}^{-1}$.

The experimental formulas are used to calculate the relaxation time [41, 42, 43]. The phonon relaxation time for phonon-phonon umklapp scattering [54, 42] is

$$\tau_U^{-1} = B_U \omega^2 T \exp(-\Theta_p/3T),$$

where $B_U = \frac{\hbar \gamma_p^2}{M \Theta_p |\mathbf{v}|^2}$. The Grvneisen parameters γ_p and Debye temperature Θ_p are $\gamma_{LA} = 2$, $\gamma_{TA} = 2/3$, $\gamma_{ZA} = -1.5$, $\Theta_{LA} = 1826.39 \text{K}$, $\Theta_{TA} = 1126.18 \text{K}$, $\Theta_{ZA} = 623.62 \text{K}$, respectively. $\bar{M} = 12 + c$ is the average mass per carbon atom, c is the abundance of ^{13}C and we set $c = 1.1\%$. The phonon relaxation time for phonon-phonon normal scattering [41, 42, 43] is

$$\tau_N^{-1} = B_N \omega^{a_N} T^{b_N},$$

where $B_N = \left(\frac{k_B}{\hbar}\right)^{b_N} \frac{\hbar \gamma_p^2 V_0^{(a_N + b_N - 2)/3}}{M |\mathbf{v}|^{a_N + b_N}}$, $V_0 = 8.769634 \times 10^{-30} \text{m}^3$ is the average volume per atom in graphene. In this study, we set $a_N = 1$, $b_N = 3$ [43]. The phonon isotope scattering [55] is

$$\tau_I^{-1} = B_p \Gamma S_0 \omega^2 D(\omega, p),$$

where $B_{ZA} = \pi/2$, $B_{LA} = B_{TA} = \pi/4$. $\Gamma = c(1 - c)/(12 + c)^2$ and $S_0 = 2.62 \times 10^{-20} \text{m}^2$ is the average area per carbon atom in graphene. Based on the Mathiessen's rule [50], we can calculate the resistive (R) scattering $\tau_R^{-1} = \tau_U^{-1} + \tau_I^{-1}$. In addition, we set $\tau^{-1} = \tau_N^{-1} + \tau_R^{-1}$.

APPENDIX C: Analytical solutions of the phonon BTE as $\text{Kn} \rightarrow 0$ or in the ballistic regime

The thermal transport in graphene disk as $\text{Kn} \rightarrow 0$ or in the ballistic regime is derived analytically based on Eq. (5). Without special statements, the phonon dispersion is not included [50, 48, 49] and we set $|\mathbf{v}| = \omega/|\mathbf{K}|$ for simplicity.

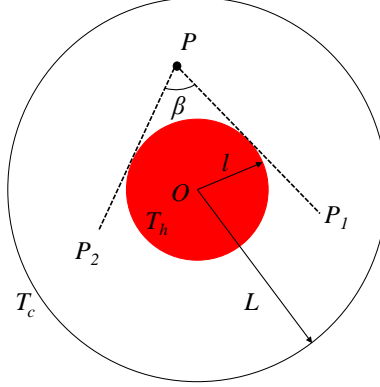


Figure 10: Geometry of the graphene disk in the ballistic limit. Lines PP_1 and PP_2 are tangent to the inner circle. $\beta = 2 \arcsin(l/r)$.

As the system size is much smaller than the phonon mean free path, the heat transfer is in the ballistic regime and there is rare phonon-phonon intrinsic scattering. Equation (5) can be written as follows approximately

$$\mathbf{v} \cdot \nabla f = 0, \quad (15)$$

which indicates that the phonon distribution function is independent of the physical position. Given a position P ($OP = r$, $l < r < L$), as shown in Fig. 10, it can be found that when all phonons with arbitrary directions transporting through P , only $\beta/2\pi \times 100\%$ come from the inner hot areas with $f_R^{eq}(T_h)$, where $\beta = 2 \arcsin(l/r)$, while the other come from the outer circle with $f_R^{eq}(T_c)$. Based on Eq. (9), the temperature at $P(r)$ can be calculated by

$$T(r) = \frac{\beta}{2\pi} T_h + \left(1 - \frac{\beta}{2\pi}\right) T_c. \quad (16)$$

Similarly, the heat flux along the radius direction is

$$\begin{aligned} \mathbf{q}(r) \cdot \mathbf{n} &= \int_0^\beta |\mathbf{v}| \cos \zeta (f_R^{eq}(T_h) - f_R^{eq}(T_c)) d\zeta \\ &= \frac{2l}{r} |\mathbf{v}| (f_R^{eq}(T_h) - f_R^{eq}(T_c)) \\ &= \frac{l}{\pi r} |\mathbf{v}| C (T_h - T_c) \end{aligned} \quad (17)$$

Then the thermal conductivity along the radius direction in the ballistic limit can be obtained by

$$\begin{aligned} k(r) &= -\frac{\mathbf{q}(r) \cdot \mathbf{n}}{dT/dr} \\ &= C |\mathbf{v}| \sqrt{(r^2 - l^2)}. \end{aligned} \quad (18)$$

At the same time, we have

$$\begin{aligned}\alpha &= \frac{\partial(\lg k^*)}{\partial r^*} \\ &= \lg\left(\frac{L}{l}\right) \times \left(1 + \frac{1}{\left(\frac{L}{l}\right)^{2r^*} - 1}\right).\end{aligned}\quad (19)$$

Actually, if considering the phonon dispersion [52, 51, 53] (appendix B), the analytical solutions of Eq. (15) in the ballistic limit are similar, i.e.,

$$T(r) = \frac{\beta}{2\pi} T_h + \left(1 - \frac{\beta}{2\pi}\right) T_c \quad (20)$$

$$\mathbf{q}(r) \cdot \mathbf{n} = \frac{l}{\pi r} (T_h - T_c) \sum_p \int (|\mathbf{v}|C) d\omega \quad (21)$$

$$k(r) = \sqrt{(r^2 - l^2)} \sum_p \int (|\mathbf{v}|C) d\omega \quad (22)$$

As the system size is much larger than the phonon mean free path, i.e., $\text{Kn} \rightarrow 0$, two situations are considered:

When all phonon-phonon scattering is momentum destroying R scattering, i.e.,

$$\mathbf{v} \cdot \nabla f = \frac{f_R^{eq} - f}{\tau_R}. \quad (23)$$

A first-order approximation is made

$$f \approx f_R^{eq} - \tau_R \mathbf{v} \cdot \nabla f_R^{eq}. \quad (24)$$

Then we have

$$\begin{aligned}\mathbf{q} &= \int_{2\pi} \mathbf{v} f d\Omega \\ &= - \int_{2\pi} \mathbf{v} \tau_R \mathbf{v} \cdot \nabla f_R^{eq} d\Omega \\ &= - \frac{\tau_R C |\mathbf{v}|^2}{2\pi} \int_{2\pi} \mathbf{s} \mathbf{s} \cdot \nabla T d\Omega \\ &= - \frac{1}{2} \tau_R C |\mathbf{v}|^2 \nabla T d\Omega \\ &= -k_{\text{bulk}} \nabla T,\end{aligned}\quad (25)$$

where $k_{\text{bulk}} = \frac{1}{2} \tau_R C |\mathbf{v}|^2$ is the bulk thermal conductivity. According to Eq. (1), we have

$$\begin{aligned}\text{constant} &= - \frac{1}{dT/d(\ln r)} \\ \implies dT &\propto d(\ln r).\end{aligned}\quad (26)$$

When all phonon-phonon scattering is momentum conservation N scattering, i.e.,

$$\mathbf{v} \cdot \nabla f = \frac{f_N^{eq} - f}{\tau_N}. \quad (27)$$

A zero-order approximation is made, i.e.,

$$f \approx f_N^{eq}. \quad (28)$$

Considering the symmetry, the direction of the drift velocity \mathbf{u} is along the radius direction, i.e., $|\mathbf{u}| = \mathbf{u} \cdot \mathbf{n}$.

When $l < r < L$, the total heat flux $Q(r)$ across the circle with radius r is

$$\begin{aligned} Q(r) &= 2\pi r \mathbf{n} \cdot \left(\int_{2\pi} \mathbf{v} f_N^{eq} d\Omega \right) \\ &= 2\pi r \mathbf{n} \cdot \left(\int_{2\pi} \mathbf{v} \frac{CT}{2\pi} \frac{|\mathbf{K}| \mathbf{s} \cdot \mathbf{u}}{\omega} \right) \\ &= CT(r) r \mathbf{n} \cdot \int_{2\pi} \mathbf{s} \mathbf{s} \cdot \mathbf{u} d\Omega, \\ &= \pi C r T(r) |\mathbf{u}(r)|. \end{aligned} \quad (29)$$

Combining the boundary conditions, i.e., Eq.(14), when $r \rightarrow l$,

$$\begin{aligned} Q(r) &= 2\pi l \mathbf{n} \cdot \left(\int_{\mathbf{s} \cdot \mathbf{n} > 0} \mathbf{v} f_R^{eq}(T_h) d\Omega + \int_{\mathbf{s} \cdot \mathbf{n} < 0} \mathbf{v} f_N^{eq} d\Omega \right) \\ &= 2lC|\mathbf{v}|T_h - 2lCT(r)|\mathbf{v}| + \frac{\pi}{2}CT(r)l|\mathbf{u}(r)|, \end{aligned} \quad (30)$$

when $r \rightarrow L$,

$$\begin{aligned} Q(r) &= 2\pi r \mathbf{n} \cdot \left(\int_{\mathbf{s} \cdot \mathbf{n} < 0} \mathbf{v} f_R^{eq}(T_c) d\Omega + \int_{\mathbf{s} \cdot \mathbf{n} > 0} \mathbf{v} f_N^{eq} d\Omega \right) \\ &= -2LC|\mathbf{v}|T_c + 2LC|\mathbf{v}|T(r) + \frac{\pi}{2}CT(r)L|\mathbf{u}(r)|. \end{aligned} \quad (31)$$

As we known, the N scattering causes no thermal resistance [15, 19, 49], which indicates that $T(r)$ is a constant along the radius direction as $\text{Kn} \rightarrow 0$. In addition, based on the energy conservation, $Q(r)$ is a constant at steady state. Combining Eqs. (29), (30) and (31), we have

$$T = \frac{lT_h + LT_c}{l + L}, \quad (32)$$

$$|\mathbf{u}(r)| = \frac{4|\mathbf{v}|lL(T_h - T_c)}{r\pi(lT_h + LT_c)}. \quad (33)$$

5. Conflict of interest

There is no conflict of interest.

Acknowledgments

This work was supported by the National Key Research and Development Plan (No. 2016YFB0600805). Chuang Zhang acknowledges Rulei Guo for useful discussions and guide.

References

References

- [1] J. Holman, *Heat transfer*. Mechanical engineering series, McGraw-Hill, 1989.
- [2] D. G. Cahill, W. K. Ford, K. E. Goodson, G. D. Mahan, A. Majumdar, H. J. Maris, R. Merlin, and S. R. Phillpot, “Nanoscale thermal transport,” *J. Appl. Phys.*, vol. 93, no. 2, pp. 793–818, 2003.
- [3] D. G. Cahill, P. V. Braun, G. Chen, D. R. Clarke, S. Fan, K. E. Goodson, P. Keblinski, W. P. King, G. D. Mahan, A. Majumdar, *et al.*, “Nanoscale thermal transport. ii. 2003–2012,” *Appl. Phys. Rev.*, vol. 1, no. 1, p. 011305, 2014.
- [4] C. W. Chang, D. Okawa, H. Garcia, A. Majumdar, and A. Zettl, “Breakdown of fourier’s law in nanotube thermal conductors,” *Phys. Rev. Lett.*, vol. 101, no. 7, p. 075903, 2008.
- [5] S. Lepri, R. Livi, and A. Politi, “Heat conduction in chains of nonlinear oscillators,” *Phys. Rev. Lett.*, vol. 78, pp. 1896–1899, Mar 1997.
- [6] G. Chen, *Nanoscale energy transport and conversion: a parallel treatment of electrons, molecules, phonons, and photons*. Oxford University Press, 2005.
- [7] A. Majumdar, “Microscale heat conduction in dielectric thin films,” *J. Heat Transf.*, vol. 115, no. 1, pp. 7–16, 1993.
- [8] R. Chen, A. I. Hochbaum, P. Murphy, J. Moore, P. Yang, and A. Majumdar, “Thermal conductance of thin silicon nanowires,” *Phys. Rev. Lett.*, vol. 101, p. 105501, Sep 2008.
- [9] D. Li, Y. Wu, P. Kim, L. Shi, P. Yang, and A. Majumdar, “Thermal conductivity of individual silicon nanowires,” *Appl. Phys. Lett.*, vol. 83, pp. 2934–2936, sep 2003.
- [10] C. Bera, N. Mingo, and S. Volz, “Marked effects of alloying on the thermal conductivity of nanoporous materials,” *Phys. Rev. Lett.*, vol. 104, p. 115502, Mar 2010.
- [11] J.-K. Yu, S. Mitrovic, D. Tham, J. Varghese, and J. R. Heath, “Reduction of thermal conductivity in phononic nanomesh structures,” *Nat. Nanotech.*, vol. 5, no. 10, pp. 718–721, 2010.
- [12] R. Anufriev, A. Ramiere, J. Maire, and M. Nomura, “Heat guiding and focusing using ballistic phonon transport in phononic nanostructures,” *Nature Commun.*, vol. 8, p. 15505, 2017.
- [13] M. Maldovan, “Phonon wave interference and thermal bandgap materials,” *Nat. Mater.*, vol. 14, no. 7, pp. 667–674, 2015.
- [14] L. Lindsay, D. A. Broido, and N. Mingo, “Flexural phonons and thermal transport in graphene,” *Phys. Rev. B*, vol. 82, p. 115427, Sep 2010.

- [15] S. Lee, D. Broido, K. Esfarjani, and G. Chen, “Hydrodynamic phonon transport in suspended graphene,” *Nat. Commun.*, vol. 6, p. 6290, 2015.
- [16] B. Qiu and X. Ruan, “Reduction of spectral phonon relaxation times from suspended to supported graphene,” *Appl. Phys. Lett.*, vol. 100, p. 193101, may 2012.
- [17] K. S. Novoselov, A. K. Geim, S. V. Morozov, D. Jiang, Y. Zhang, S. V. Dubonos, I. V. Grigorieva, and A. A. Firsov, “Electric field effect in atomically thin carbon films,” *Science*, vol. 306, no. 5696, pp. 666–669, 2004.
- [18] A. K. Geim and K. S. Novoselov, “The rise of graphene,” *Nat. Mater.*, vol. 6, no. 3, pp. 183–191, 2007.
- [19] A. Cepellotti, G. Fugallo, L. Paulatto, M. Lazzeri, F. Mauri, and N. Marzari, “Phonon hydrodynamics in two-dimensional materials,” *Nat. Commun.*, vol. 6, no. 1, 2015.
- [20] S. Huberman, R. A. Duncan, K. Chen, B. Song, V. Chiloyan, Z. Ding, A. A. Maznev, G. Chen, and K. A. Nelson, “Observation of second sound in graphite at temperatures above 100 K,” *Science*, p. eaav3548, 3 2019.
- [21] O. Narayan and S. Ramaswamy, “Anomalous heat conduction in one-dimensional momentum-conserving systems,” *Phys. Rev. Lett.*, vol. 89, no. 20, p. 200601, 2002.
- [22] S. Lepri, R. Livi, and A. Politi, “Thermal conduction in classical low-dimensional lattices,” *Phys. Rep.*, vol. 377, no. 1, pp. 1 – 80, 2003.
- [23] D. Lacroix, K. Joulain, and D. Lemonnier, “Monte carlo transient phonon transport in silicon and germanium at nanoscales,” *Phys. Rev. B*, vol. 72, p. 064305, Aug 2005.
- [24] C. Zhang and Z. Guo, “Discrete unified gas kinetic scheme for multiscale heat transfer with arbitrary temperature difference,” *Int. J. Heat Mass Transfer*, vol. 134, pp. 1127–1136, 2019.
- [25] A. J. Markworth, K. S. Ramesh, and W. P. Parks, “Modelling studies applied to functionally graded materials,” *J. Mater. Sci.*, vol. 30, no. 9, pp. 2183–2193, 1995.
- [26] G. D. Mahan, “Inhomogeneous thermoelectrics,” *J. Appl. Phys.*, vol. 70, pp. 4551–4554, 10 1991.
- [27] K. M. Liew, S. Kitipornchai, X. Z. Zhang, and C. W. Lim, “Analysis of the thermal stress behaviour of functionally graded hollow circular cylinders,” *Int. J. Solids Struct.*, vol. 40, pp. 2355–2380, 5 2003.
- [28] C. W. Chang, D. Okawa, A. Majumdar, and A. Zettl, “Solid-state thermal rectifier,” *Science*, vol. 314, no. 5802, pp. 1121–1124, 2006.
- [29] B. Li, L. Wang, and G. Casati, “Thermal diode: Rectification of heat flux,” *Phys. Rev. Lett.*, vol. 93, no. 18, p. 184301, 2004.

- [30] N. Yang, G. Zhang, and B. Li, “Carbon nanocone: A promising thermal rectifier,” *Appl. Phys. Lett.*, vol. 93, no. 24, p. 243111, 2008.
- [31] N. Yang, G. Zhang, and B. Li, “Thermal rectification in asymmetric graphene ribbons,” *Appl. Phys. Lett.*, vol. 95, p. 033107, jul 2009.
- [32] Z. Wang, R. Zhao, and Y. Chen, “Monte carlo simulation of phonon transport in variable cross-section nanowires,” *Sci. China Technol. Sci.*, vol. 53, no. 2, pp. 429–434, 2010.
- [33] N. Yang, S. Hu, D. Ma, T. Lu, and B. Li, “Nanoscale Graphene Disk: A Natural Functionally Graded Material—How is Fourier’s Law Violated along Radius Direction of 2d Disk,” *Sci. Rep.*, vol. 5, p. 14878, 2015.
- [34] D. Ma, H. Ding, X. Wang, N. Yang, and X. Zhang, “The unexpected thermal conductivity from graphene disk, carbon nanocone to carbon nanotube,” *Int. J. Heat Mass Transfer*, vol. 108, pp. 940 – 944, 2017.
- [35] Y. Guo and M. Wang, “Heat transport in two-dimensional materials by directly solving the phonon Boltzmann equation under callaway’s dual relaxation model,” *Phys. Rev. B*, vol. 96, p. 134312, Oct 2017.
- [36] J. Callaway, “Model for lattice thermal conductivity at low temperatures,” *Phys. Rev.*, vol. 113, pp. 1046–1051, Feb 1959.
- [37] Z. Ding, J. Zhou, B. Song, V. Chiloyan, M. Li, T.-H. Liu, and G. Chen, “Phonon hydrodynamic heat conduction and knudsen minimum in graphite,” *Nano Lett.*, vol. 18, no. 1, pp. 638–649, 2018. PMID: 29236507.
- [38] V. A. Fiveland and J. P. Jessee, “Acceleration schemes for the discrete ordinates method,” *J. Thermophys. Heat Transfer.*, vol. 10, no. 3, pp. 445–451, 1996.
- [39] M. L. Adams and E. W. Larsen, “Fast iterative methods for discrete-ordinates particle transport calculations,” *Prog. Nucl. Energ.*, vol. 40, no. 1, pp. 3 – 159, 2002.
- [40] C. Zhang, Z. Guo, and S. Chen, “Unified implicit kinetic scheme for steady multiscale heat transfer based on the phonon Boltzmann transport equation,” *Phys. Rev. E*, vol. 96, p. 063311, Dec 2017.
- [41] A. S. Nissimagoudar and N. S. Sankeshwar, “Significant reduction of lattice thermal conductivity due to phonon confinement in graphene nanoribbons,” *Phys. Rev. B*, vol. 89, p. 235422, Jun 2014.
- [42] D. T. Morelli, J. P. Heremans, and G. A. Slack, “Estimation of the isotope effect on the lattice thermal conductivity of group iv and group iii-v semiconductors,” *Phys. Rev. B*, vol. 66, p. 195304, Nov 2002.

- [43] A. K. Majee and Z. Aksamija, “Length divergence of the lattice thermal conductivity in suspended graphene nanoribbons,” *Phys. Rev. B*, vol. 93, p. 235423, Jun 2016.
- [44] N. Mingo and D. A. Broido, “Carbon nanotube ballistic thermal conductance and its limits,” *Phys. Rev. Lett.*, vol. 95, p. 096105, Aug 2005.
- [45] D. L. Nika, E. P. Pokatilov, A. S. Askerov, and A. A. Balandin, “Phonon thermal conduction in graphene: Role of umklapp and edge roughness scattering,” *Phys. Rev. B*, vol. 79, p. 155413, Apr 2009.
- [46] R. A. Guyer and J. A. Krumhansl, “Thermal conductivity, second sound, and phonon hydrodynamic phenomena in nonmetallic crystals,” *Phys. Rev.*, vol. 148, pp. 778–788, Aug 1966.
- [47] R. J. Hardy, “Phonon Boltzmann equation and second sound in solids,” *Phys. Rev. B*, vol. 2, pp. 1193–1207, Aug 1970.
- [48] X. Li and S. Lee, “Crossover of ballistic, hydrodynamic, and diffusive phonon transport in suspended graphene,” *Phys. Rev. B*, vol. 99, p. 085202, Feb 2019.
- [49] R. Yang, S. Yue, and B. Liao, “Hydrodynamic phonon transport perpendicular to diffuse-gray boundaries,” *Nanosc. Microsc. Therm.*, vol. 23, no. 1, pp. 25–35, 2019.
- [50] J. Y. Murthy, S. V. J. Narumanchi, J. A. Pascual-Gutierrez, T. Wang, C. Ni, and S. R. Mathur, “Review of multiscale simulation in submicron heat transfer,” *Int. J. Multiscale Computat. Eng.*, vol. 3, no. 1, pp. 5–32, 2005.
- [51] E. Pop, V. Varshney, and A. K. Roy, “Thermal properties of graphene: Fundamentals and applications,” *MRS Bull.*, vol. 37, no. 12, pp. 1273–1281, 2012.
- [52] L. Wirtz and A. Rubio, “The phonon dispersion of graphite revisited,” *Solid State Commun.*, vol. 131, no. 3, pp. 141 – 152, 2004.
- [53] K. S. Novoselov, A. K. Geim, S. V. Morozov, D. Jiang, Y. Zhang, S. V. Dubonos, I. V. Grigorieva, and A. A. Firsov, “Electric Field Effect in Atomically Thin Carbon Films,” *Science*, vol. 306, pp. 666–669, Oct. 2004.
- [54] Z. Aksamija and I. Knezevic, “Lattice thermal conductivity of graphene nanoribbons: Anisotropy and edge roughness scattering,” *Appl. Phys. Lett.*, vol. 98, no. 14, p. 141919, 2011.
- [55] L. Lindsay, W. Li, J. Carrete, N. Mingo, D. A. Broido, and T. L. Reinecke, “Phonon thermal transport in strained and unstrained graphene from first principles,” *Phys. Rev. B*, vol. 89, p. 155426, Apr 2014.